PCCP

On the Measurement of Relaxation Times of Acoustic Vibrations in Metal Nanowires

Journal:	*Physical Chemistry Chemical Physics*
Manuscript ID	CP-ART-05-2018-003230.R1
Article Type:	Paper
Date Submitted by the Author:	13-Jun-2018

Complete List of Authors:	Devkota, Tuphan; University of Notre Dame, Department of Chemistry and Biochemistry Chakraborty, Debadi; University of Melbourne, Department of Mathematics and Statistics Yu, Kuai; Shenzhen University, Beane, Gary; University of Notre Dame, Department of Chemistry and Biochemistry Sader, John; The University of Melbourne, ARC Centre of Excellence in Exciton Science, School of Mathematics and Statistics Hartland, Gregory; University of Notre Dame, Department of Chemistry and Biochem

On the Measurement of Relaxation Times of Acoustic Vibrations in Metal Nanowires[†]

Tuphan Devkota,[a] Debadi Chakraborty,[b] Kuai Yu,[c] Gary Beane,[a] John E. Sader,[b] and Gregory V. Hartland[a,‡]

[a] *Department of Chemistry and Biochemistry, University of Notre Dame, Notre Dame, Indiana 46556, United States*

[b] *ARC Centre of Excellence in Exciton Science, School of Mathematics and Statistics, The University of Melbourne, Victoria 3010, Australia*

[c] *College of Electronic Science and Technology, Shenzhen University, Shenzhen, 518060, P. R. China*

---

† Electronic Supporting Information (ESI) available: Continuum mechanics expressions for vibrational frequencies and quality factors of cylindrical nanowires, description of finite element simulations, experimental quality factors for the suspended and supported nanowires in different environments, and changes in vibrational frequencies upon addition of liquid.

‡ Corresponding author: e-mail ghartlan@nd.edu; telephone (574) 631-9320

Abstract:

The mechanical resonances of metal nanostructures are strongly affected by their environment. In this paper the way the breathing modes of single metal nanowires are damped by liquids with different viscosities was studied by ultrafast pump-probe microscopy experiments. Both nanowires supported on a glass substrate and nanowires suspended over trenches were investigated. The measured quality factors for liquid damping for the suspended nanowires are in good agreement with continuum mechanics calculations for an inviscid fluid that assume continuity of stress and strain at the nanowire-liquid interface. This shows that liquid damping is controlled by radiation of sound waves into the medium. For the nanowires on the glass surface the quality factors for liquid damping are approximately 60% higher than those for the suspended nanowires. This is attributed to a shadowing effect. The nanowires in our measurements have pentagonal cross-sections. This produces two different breathing modes and also means that one of the faces for the supported nanowires is blocked by the substrate, which reduces the amount of damping from the liquid. Comparing the supported and suspended nanowires also allows us to estimate the effect of the substrate on the acoustic mode damping. We find that the substrate has a weak effect, which is attributed to poor mechanical contact between the nanowires and the substrate.

Introduction:

Understanding how the properties of materials change with dimensions has been a major area of research in physical chemistry for the past several decades.[1-4] For metal nanostructures the way the optical and vibrational resonances depend on size and shape has been extensively studied.[5-9] The interaction of the particles with their environment is also of interest.[9, 10] For example, it was recently shown that the emergence of viscoelastic effects in the surrounding liquid can cause a size dependence in the damping of the vibrational resonances.[11] The strength of this effect depends on the form of the vibrational mode and the Deborah number for the liquid: $\mathrm{De} = \omega\tau$, where ω is the frequency of the vibration and τ is the relaxation time of the liquid.[11-17] For vibrations that generate shear waves in the surroundings, such as the extensional modes of nanorods, viscoelastic effects in acoustic mode damping are important.[11-17] However, for breathing modes which generate compressional waves, the conditions for observing viscoelastic effects are more restrictive, and involve the viscosity, speed of sound and density of the liquid, in addition to ω and τ.[11]

In this paper the damping of the breathing modes of single gold nanowires was measured for a series of liquids by ultrafast pump-probe microscopy experiments.[16, 18-20] The lifetimes of the breathing modes were measured in air and liquid, and the difference between these two experiments was used to determine the contribution from the liquid to the damping.[14, 16, 18, 21] The nanowires in these experiments have vibrational frequencies ranging from 40 to almost 100 GHz, which are amongst the highest that have been studied to date.[9] The high frequencies produce larger Deborah numbers for a given liquid and, potentially, facilitate the observation of viscoelastic effects.[14-17] The liquids examined were water, and a series of related ionic liquids.

Ionic liquids were chosen for this study because they are available with a very wide range of viscosities, while maintaining similar densities and speeds of sound.[22]

Both nanowires supported on a glass substrate and nanowires suspended over trenches were examined.[16, 18, 23, 24] The results from the experiments show that the liquid damping for the suspended nanowires is very close to that expected for an inviscid fluid, i.e., energy flow is controlled by radiation of sound waves into the fluid.[9, 18] For the supported nanowires the quality factors for liquid damping are approximately 60% larger than those for the suspended nanowires (that is, the liquid has a smaller effect on energy relaxation). This is attributed to a blocking effect from the substrate, which reduces the relative amount of the nanowire surface exposed to the liquid and, therefore, the contribution of the liquid to the damping. By comparing the damping for the supported and suspended nanowires in air we also obtained an estimate of the contribution from the substrate to the damping. The results show that the substrate has only a small effect on damping. This is attributed to poor mechanical contact between the nanowire and the substrate. These results are important for understanding energy dissipation in nanomaterials and, potentially, for the development of mass sensors based on the vibrational response of nanomaterials.[25, 26]

Experimental Methods:

The single nanowire pump-probe measurements were performed using a Chameleon Ultra II Ti:Sapphire laser (80 MHz repetition rate) operating at 720 nm.[27] The output of the laser was split by a 90:10 beam splitter, and the intense portion was used to pump a Mira OPO to produce 530 nm pulses, which were used as the probe beam. The 10% portion of the Chameleon output was used as the pump beam. The 530 nm probe wavelength was chosen because this

wavelength is resonant with the transverse plasmon band on the nanowires.[18] The two beams were combined with a dichroic mirror, and were focused tightly onto the sample using a high NA oil immersion objective (Olympus UPlanFLN, 100x/NA=1.3). The transmitted beams were collected with a second high NA objective. After filtering out the pump beam, the probe beam was focused onto a Hamamatsu C5331-11 avalanche photodiode. The typical powers used were 70 μW for the probe and 180 μW for the pump before the objective. The pump beam was modulated using an acousto-optic modulator (IntraAction) at a frequency of 400 kHz and the signal was extracted using a lock-in amplifier (Stanford Research Systems SR844). A Thorlabs DDS600 delay stage was used to control the timing between the pump and probe pulses. Time-resolved traces were measured by collecting the lock-in signal as a function of delay time.

Au nanowires with nominal 30 nm average diameter and 6 μm average length were obtained from Sigma-Aldrich, and nanowires with a nominal 75 nm diameter were obtained from Nanopartz. The ionic liquids 1-butyl-3-methylimidazolium hexaflurophosphate (bmim-PF_6), 1-butyl-3-methylimidazolium trifluro-methanesulfonate (bmim-OFT) and 1-butyl-3-methylimidazolium bis(triflurомethylsulfonyl)-imide (bmim-Ntf_2) were purchased from Sigma Aldrich. The viscosities and acoustic impedances of the liquids used in these experiments are listed in **Table 1**. The nanowire samples contain an excess of surfactant (hexadecylcetyltrimethylammonium bromide, CTAB), which stabilizes the solutions. To prepare the samples for the pump-probe microscopy experiments, the nanowires were washed two times with Milli-Q water by centrifugation to remove excess CTAB. A drop of the cleaned nanowire sample was then allowed to dry overnight onto a glass coverslip with trenches that were created using photolithography and reactive ion etching. This procedure creates a random distribution of nanowires over the surface, with the majority lying on the substrate ("supported nanowires") and

some nanowires spanning the trenches ("suspended nanowires"). Both suspended and supported nanowires were examined in the ultrafast pump-probe microscopy experiments in this paper. For the thinner nanowires the pump-probe experiments were performed in water first. This was because it is difficult to find these wires in scattered light images for the samples in air (adding liquid to the sample reduces the scattering from the substrate via index matching). Once their locations were known, the measurements were repeated for the nanowires in air and in the ionic liquids.[16, 18, 28] For the thicker nanowires, the measurements were performed in air first, and then in the different liquids (note that the nanowire samples were reused after the water measurements, but not after the ionic liquid measurements).

Table 1: Viscosities (μ, cP) and acoustic impedance ($Z = \rho \times c_l$, 10^6 kg m^{-2} s^{-1}) of the liquids used for pump-probe microscopy measurements taken from Refs. [22, 29, 30].

Medium	μ	Z
Water	0.89	1.49
bmim-OFT	77	1.85
bmim-Ntf_2	141	1.77
bmim-PF_6	376	1.95

The average frequency for the breathing modes for the thinner nanowires was $\langle f \rangle$ = 79 ± 9 GHz (error equal standard deviations). Comparison of the measured frequency to continuum mechanics calculations of the breathing mode frequencies of a infinite cylinder (see the Supplemental Information for details) implies an average diameter of 32 ± 3 nm,[18] which is consistent with the size specified for this sample. However, for the nominally 75 nm sample the measured average frequency of $\langle f \rangle$ = 59 ± 9 GHz corresponds to an average diameter of 45 ± 7 nm, which is considerably different than the specified width. This could be due to actual differences in the size distribution of the sample, or because of a selection bias in the

experiments. The discrepancy between the specified and estimated diameter of the larger nanowires is not important for this study.

The effect of organic molecules at the surface of the nanowires was also examined by recording pump-probe traces for the nominally 75 nm diameter nanowires before and after cleaning by an oxygen plasma (Harrick Plasma Cleaner, PDC-32G, 20 minutes). The larger nanowires where used for these experiments because plasma cleaning rearranges the thinner nanowires on the substrate.

Results and Discussion:

Figure 1(a) shows representative pump-probe traces for a suspended nanowire in air and water. The pump-probe signal shows an initial fast decay, which corresponds to the rapid cooling of the excited electrons through electron-phonon coupling.[10] The slower oscillating signal observed after several picoseconds delay is due to the breathing mode vibrations in the nanowire. These vibrations are impulsively excited by the fast heating of the nanowire lattice induced by the electron-phonon coupling process.[10, 28, 31] The nanowires used in this study have a pentagonal cross-section and, thus, show two breathing modes.[18] One mode corresponds to motion at the apexes of the pentagon and the other to motion at the faces (see below).[16, 18] After the initial fast decay, the pump-probe traces can be fit with the function $a + b\, e^{-t/\tau} + \sum_{i=1,2} c_i \cos(2\pi f_i t + \phi_i) e^{-t/\tau_i}$ (red line in **Figure 1(a)**), where the first two terms account for the background signal and the two damped cosine functions correspond to the two vibrational modes of the nanowire. The fit yields the frequencies f_i and lifetimes τ_i of the breathing mode vibrations. The errors from this fitting procedure are typically on the order of 0.2% for the frequencies and 10% for the lifetimes. Note that there is a negligible change in frequency when

liquid is added to the samples – see the Supporting Information for more details. Our previous studies have shown that there is no significant difference in the damping for the two breathing modes.[16] Thus, in the analysis presented below the data for these two modes were simply averaged together.

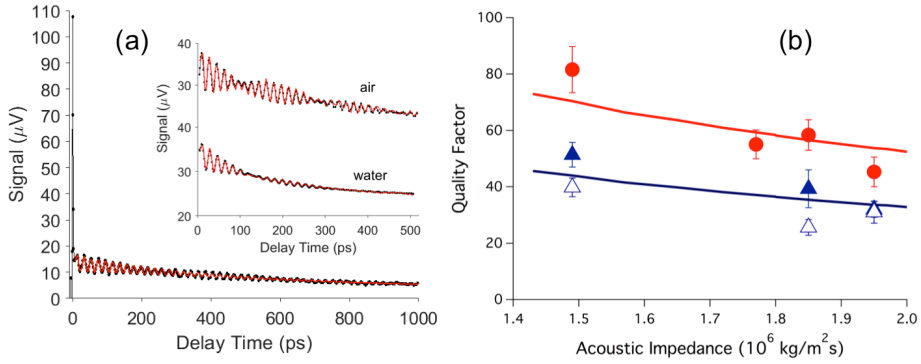

Figure 1: (a) Pump-probe traces for a single supported nanowire in air and water. The red lines show a fit to the data using the damped (double) cosine function described in the text. (b) Average quality factors for liquid damping measured for suspended (blue markers) and supported nanowires (red markers) versus acoustic impedance. The open symbols correspond to the larger nanowire sample. The error bars on the markers are 95% confidence limits. The solid blue line is the calculated quality factors for a cylindrical nanowire in an inviscid liquid, and the red line is the calculated quality factor multiplied by 1.6.

To compare the damping for different nanowires, the lifetimes are expressed in terms of quality factors $Q_i = \pi f_i \tau_i$. This removes the trivial size dependence that arises from the way the lifetimes and periods scale with size.[32-34] For a metal nanowire the damping of the acoustic modes has contributions from several sources: internal damping from the metal, energy dissipation into the substrate (for the supported nanowires), damping from surfactant at the

surface of the nanowire, and damping from the liquid. In terms of quality factors the different contributions add as:[12, 13, 18, 21, 28, 35, 36]

$$\frac{1}{Q_{tot}} = \frac{1}{Q_{int}} + \frac{1}{Q_{sub}} + \frac{1}{Q_{surf}} + \frac{1}{Q_{liq}} \quad (1)$$

where Q_{int}, Q_{sub}, Q_{surf} and Q_{liq} denote the effects from internal damping, the substrate, surface bound molecules and the liquid, respectively. The effects from the liquid can be isolated by performing a reference experiment for the nanowires in air, and comparing the results to the nanowires in the liquid.[16, 18, 21] For the suspended nanowires the quality factor for the reference measurements is $Q_{ref}^{-1} = Q_{int}^{-1} + Q_{surf}^{-1}$, whereas, for the supported nanowires there is an extra contribution from the substrate: $Q_{ref}^{-1} = Q_{int}^{-1} + Q_{surf}^{-1} + Q_{sub}^{-1}$. In both cases the difference between the liquid and air measurements gives the effect of the liquid: $Q_{liq}^{-1} = Q_{tot}^{-1} - Q_{ref}^{-1}$. In the experiments described below, we obtained values of Q_{liq} for the individual nanowires and then averaged the results.[16] This allows us to calculate a standard deviation and, thus, the 95% confidence limit for $\langle Q_{liq} \rangle$, which is important for determining the accuracy of the measurements.

The average quality factors determined for liquid damping are presented in **Table 2** for the supported and suspended nanowires, along with the 95% confidence limits for the measurements. Before discussing the liquid damping data we first note that, counter to our intuition, the substrate has only a minor effect on the damping of the acoustic modes. Specifically, averaging all the measurements for the nominally 30 nm diameter sample we find $\langle Q_{air} \rangle = 34 \pm 3$ for the suspended nanowires, and $\langle Q_{air} \rangle = 30 \pm 3$ for the supported nanowires (errors equal 95% confidence limits). Pump-probe microscopy studies of lithographically fabricated nanostructures on surfaces typically show significantly smaller quality factors, on the order of 10 – 20,[37-40] than those measured here for the supported nanowires. This is often

interpreted to mean that the nanostructures suffer from strong substrate damping.[21, 37-41] However, a recent study of gold nanodisks fabricated by e-beam lithography demonstrated that internal damping was the dominant relaxation channel, and that the substrate has a minor effect.[42] The quality factor for damping by the substrate in our experiments can be estimated from the $\langle Q_{air} \rangle$ values for the supported and suspended nanowires by $\langle Q_{sub} \rangle^{-1} = \langle Q_{air}^{supported} \rangle^{-1} - \langle Q_{air}^{suspended} \rangle^{-1}$, see Equation (1). This analysis yields $\langle Q_{sub} \rangle = 240 \pm 40$, which is a rather small effect, consistent with the conclusions of Ref. [42]. The weak substrate effect will be discussed in more detail below.

The effect of the surfactant layer on the damping was also investigated. The quality factor for the surfactant Q_{surf} was measured by recording data for suspended nanowires from the nominally 75 nm diameter sample before and after exposure to an oxygen ion plasma - which removes the organic CTAB layer from the sample. It was observed that the quality factors for the nanowires in air increase from $\langle Q_{air} \rangle = 37 \pm 4$ to $\langle Q_{air} \rangle = 41 \pm 5$ after plasma cleaning. Analysis of the data using Equation (1) gives a value of $\langle Q_{surf} \rangle = 310 \pm 70$ for the surfactant layer coating the nanowires, which is similar to the damping from the substrate. This estimate of the effect of the CTAB layer is consistent with the results in Ref. [16].

Table 2: Average values of the vibrational frequencies $\langle f_{air} \rangle$ and total quality factors $\langle Q_{air} \rangle$ in air, and quality factors for liquid damping $\langle Q_{liq} \rangle$ for suspended and supported gold nanowires. The errors for $\langle Q \rangle$ represent 95% confidence limits, and the errors for $\langle f \rangle$ are standard deviations.

Sample	Medium	$\langle f_{air} \rangle$	$\langle Q_{air} \rangle$	$\langle Q_{liq} \rangle$
Supported - small	Water	79 ± 9	30 ± 3	82 ± 8
	bmim-OFT			58 ± 5

	bmim-Ntf_2			55 ± 5
	bmim-PF_6			45 ± 5
Suspended - small	Water	79 ± 9	34 ± 3	51 ± 4
	bmim-OFT			39 ± 7
	bmim-PF_6			32 ± 3
Suspended - large	Water	59 ± 9	38 ± 3	40 ± 3
	bmim-OFT			26 ± 4
	bmim-PF_6			31 ± 4

The data for both the supported and the suspended nanowires in **Table 2** shows that the values of Q_{liq} decrease with increasing liquid viscosity. However, the changes in Q_{liq} are relatively modest compared to the changes in viscosity. For example, the measured values of Q_{liq} change by less than a factor of 2 for water compared to bmim-PF_6, whereas the viscosities change by a factor of ~ 400 (see **Table 1**). The changes in Q_{liq} are also correlated with the changes in the acoustic impedance ($Z = \rho \times c_l$) of the liquids, which is the important factor for inviscid fluid flow.[11, 14, 15, 17] **Figure 1(b)** shows a plot of $\langle Q_{liq} \rangle$ for the supported and suspended nanowires versus the acoustic impedance. The solid blue line is the quality factor calculated for cylindrical gold nanowires with circular cross-sections using the model for damping described in Refs. [18, 28], which is appropriate for an inviscid liquid.[11] In this calculation the nanowire is modeled as an infinitely long cylinder in a homogeneous medium, with continuity in the strain and radial stress at the nanowire surface.[43-45] Damping occurs by radiation of sound waves into the surroundings, the efficiency of which depends on the difference in acoustic impedance between the nanowire and the surroundings, see the Supplemental Information for more details.[21, 32, 41, 46] The calculations are in reasonable agreement with the data for the suspended nanowires, which implies that radiation of sound waves into the surroundings (inviscid fluid flow) is the dominant effect in these experiments. This observation is consistent with the theory for viscoelastic effects in nanoparticle fluid interactions derived in Ref. [11], where it was shown

that vibrations that generate compressional waves, such as the breathing modes studied here, do not trigger a viscoelastic response in the surrounding medium.

The quality factors for liquid damping for the supported nanowires are approximately 60% higher than the values for the suspended nanowires, see **Table 2** and the red line in **Figure 1(b)**. The increase in $\langle Q_{liq} \rangle$ for the supported nanowires compared to the suspended nanowires can be understood from a simple geometric argument.[21] The nanowires in our experiments have roughly pentagonal cross-sections. When they are placed on a surface not all the faces are exposed to the environment (one is protected by the surface). Thus, when the liquid is added to the sample it only affects 4 of the 5 faces, which reduces the effect of the liquid on the vibrational damping.[21] Intuitively we would expect Q_{liq} to be increased by a factor of 5/4 for the supported nanowires compared to the suspended nanowires (the ratio of the number of exposed faces for a pentagonal nanowire over a trench compared to on a surface). Experimentally we observe a factor of 1.6 ± 0.1, which is consistent with the idea of a "shadowing effect" from the surface.

To test the scaling argument presented above for the shadowing effect, finite element simulations were performed for a pentagonal nanowire with different numbers of faces immersed in water. The simulations were performed by implementing compressible viscoelastic constitutive equations in the eigenfrequency solver of COMSOL Multiphysics, as described in detail in Ref. [[17]]. **Figure 2(a)** shows a diagram of the simulation model. The simulations were performed in two-dimensions and thus correspond to the physical case where the length of the nanowire is much larger than the lateral dimensions. The pentagonal nanowires show two breathing modes (see below), which have slightly different liquid damping quality factors. The markers in **Figure 2(b)** show the simulated quality factors for the breathing modes plotted versus

$1/n$, where n is the number of faces in contact with the water. The lines show the quality factor for liquid damping calculated by $Q_{liq}^{n-faces} = 5Q_{liq}/n$, where Q_{liq} is the damping for a completely submerged nanowire. The good agreement between the simulations and the $1/n$ scaling relation supports the simple idea that liquid damping for partially submerged nanostructures just depends on the relative surface area exposed to the liquid.[21]

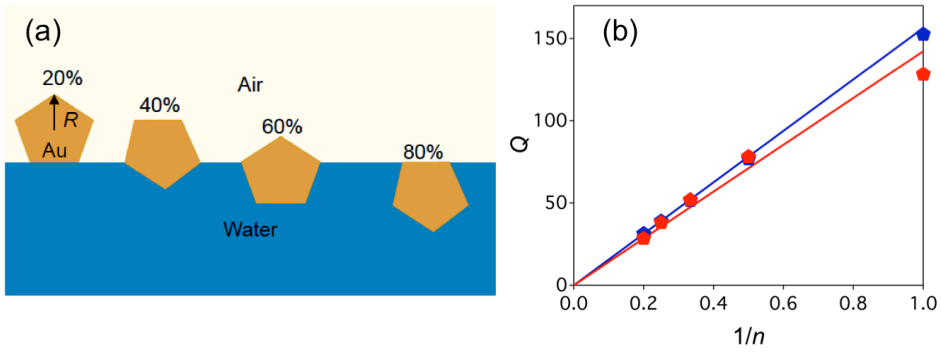

Figure 2: (a) Schematic diagram of the simulation model for a partially submerged pentagonal nanowire. The numbers give the percentage of the nanowire surface covered by water. (b) Quality factors for liquid damping for a pentagonal nanowire with a 30 nm diameter with different numbers of faces (n) in contact with the liquid plotted versus $1/n$. The blue symbols and line are for the high frequency breathing mode, and red symbols and line are for the low frequency mode.

We now compare the measured quality factor for substrate damping of $\langle Q_{sub} \rangle = 240 \pm 40$ to calculated values. First, we use the quality factors from the analytic model for an infinitely long cylindrical nanowire in a homogeneous medium described above,[18] and scale the results by the relative amount of surface area in contact with the substrate (as was done in the analysis in **Figure 2**). Using an acoustic impedance of $Z_{glass} = 14.5\times10^6$ kg m^{-2} s we obtain $Q_{glass} = 4.8$ for a Au nanowire completely surrounded by glass. The quality factor for a pentagonal nanowire

on a glass substrate is then estimated as $Q_{sub} = (5/1) \times Q_{glass} = 24$. This crude estimate of Q_{sub} is an order of magnitude smaller than the experimental measurement. However, this analysis does not include the surfactant layer present on the nanowire, or properly account for the form of the breathing modes for the pentagonal nanowires in our experiments.

To obtain a more sophisticated estimate of the substrate effect, we use finite element simulations. The eigenfrequency calculations in **Figure 2** are difficult to perform for nanostructures in contact with a solid surface. Thus, simulations for the supported nanowires were performed using a frequency domain calculation in the Solid Mechanics model of COMSOL Multiphysics. A two-dimensional model was used which, again, implies an infinitely long nanowire. This calculation yields the vibrational eigenvalues of all the normal modes of the system. **Figure 3(a)** shows a plot of the expected contributions from the different modes of a free 30 nm diameter pentagonal nanowire (no substrate) to the pump-probe signal. The amplitudes were calculated by projecting the dilation of the normal modes onto the initial displacement of the nanowire - which is isotropic expansion.[44, 47, 48] The response is dominated by the breathing modes of the nanowire, and the insets in **Fig. 3(a)** show the form of the two breathing modes determined from the finite element simulations. **Figures 3(b)** and **3(c)** show analogous calculations for a supported nanowire on a glass surface, with and without a layer of organic material between the glass and the metal (to model the CTAB layer of the nanowires). For the supported nanowire the mode projection calculations were performed by only integrating over the domain of the nanowire. This picks out the modes that cause a significant volume change in the nanowire, which are the ones detected in the pump-probe measurements.

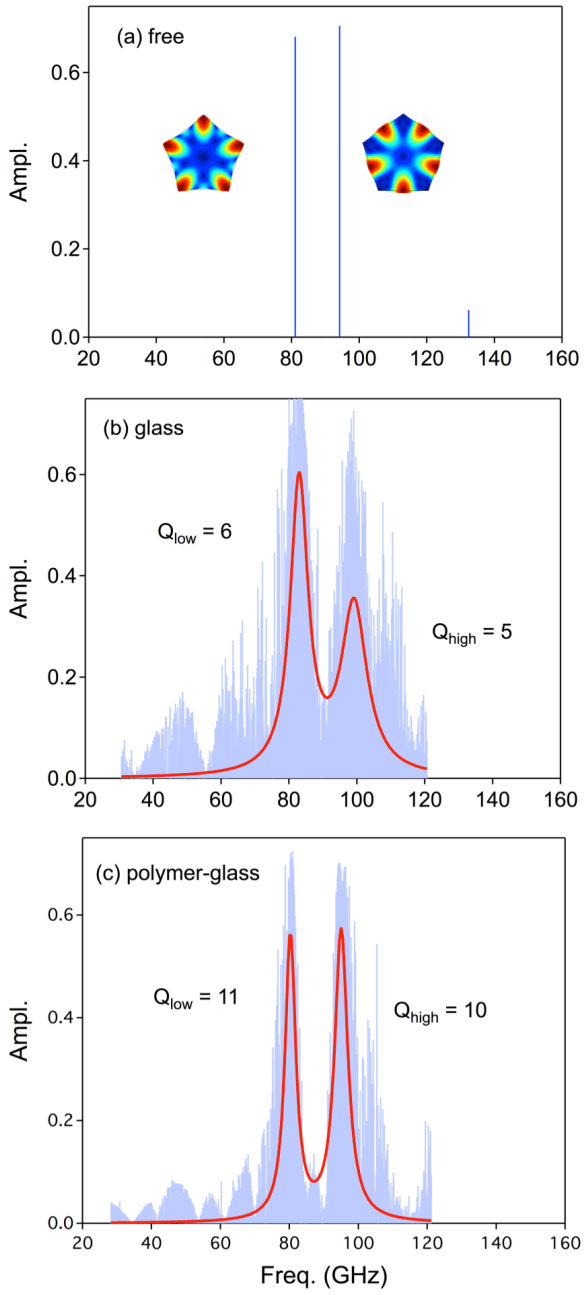

Figure 3: (a) Mode analysis calculations for a free pentagonal nanowire with a diameter of 30 nm. The amplitude is the projection of the normal mode onto the initial displacement of the nanowire induced by laser heating. Analogous calculations for the nanowire on a solid glass surface and on a surface with a 4 nm thick layer of organic material between the nanowire and the glass are shown in panels (b) and (c), respectively. The insets in panel (a) shows the form of

the two breathing modes that dominate the response, and the insets in panels (b) and (c) show the quality factors for the two modes when the nanostructure is in contact with a surface.

The results in **Figures 3(b)** and **3(c)** show that the break in symmetry due to the surface hybridizes the breathing modes of the nanowire with substrate modes.[49] This mixing broadens the spectral lines, which is the frequency domain manifestation of increased damping. Fitting the data to a double Lorentzian function $F(\nu) = \sum_i A_i\gamma_i/\{(\nu - f_i)^2 + (\gamma_i/2)^2\}$ gives quality factors for substrate damping of $Q_{sub} = f/2\gamma \approx 6$ for nanowires in direct contact with the glass, and $Q_{sub} \approx 10$ when the nanowires are separated from the glass by an organic layer.[50] This analysis shows that the surfactant layer around the nanowires has an insulating effect on the system, leading to less efficient acoustic energy flow from the nanowire to the substrate. However, the predicted magnitude of substrate damping is much larger than the experimental measurement.

Note that using a larger substrate in the simulations gives a larger density of hybridized modes, but doesn't significantly change the form of the spectrum. The width and height of the substrate used for the simulations in **Figure 3** were 1200 nm and 600 nm, respectively, and the calculated quality factors are stable to within 10% with respect to changing the dimensions of the substrate. The quality factors for the organic-glass interface simulations in **Figure 3(c)** are also not particularly sensitive to the exact values of the elastic modulus and density of the organic layer (the specific values used in **Fig. 3(c)** were E = 3 GPa, ρ = 1000 kg/m^3 and ν = 0.4). The increase in quality factor with the introduction of an organic layer between the nanowire and the glass substrate is an acoustic impedance miss-match effect. The acoustic impedance of the organic layer is much smaller than that of the glass, which means that transmission of acoustic

energy is less effective from the Au nanowire to the organic layer than from Au to glass.[21, 41, 50, 51]

We believe that the most likely explanation for the difference between the experimental and calculated values of Q_{sub} is poor contact between the nanowire and the substrate.[21, 41, 50, 51] Both the finite element simulations and the analytic calculations assume continuity in stress and strain at the different interfaces (gold-glass, gold-organic and organic-glass). However, this may not be realized in the experiments: poor mechanical contact between the nanowire and the substrate would reduce the damping effect from the substrate.[21, 37, 42, 51] In contrast to the results for the nanowires in contact with a solid surface, the calculations for liquid damping are in good agreement with the experimental results – see **Figure 1(b)**. This indicates that much better mechanical contact is created between the nanowires and liquids, so that the boundary conditions of continuity in stress and strain are better realized. Obtaining an accurate description of the boundary conditions for acoustic energy flow across solid-solid interfaces is thus a major challenge in this area of science.

Summary and Conclusions:

Overall, the results from this study demonstrate a number of subtle effects in the damping of the acoustic modes of metal nanostructures. First, for suspended nanowires the quality factors for liquid damping are close to the values calculated for an inviscid fluid. This implies that radiation of sound waves into the liquid is the dominant effect in liquid damping for the breathing modes of metal nanowires, even for high viscosity liquids like bmim-PF_6.[11, 18, 28, 32] The absence of viscoelastic effects in this system is consistent with the theory of Ref. [[11]], where

it was shown that the breathing modes of nanostructures generate an inviscid compressible fluid flow in viscoelastic liquids, that is, conventional sound wave radiation.

The pump-probe experiments also show that the liquid damping effect is much smaller (larger Q values) for supported nanowires compared to suspended nanowires. This is attributed to a shadowing effect[21] – chemically synthesized nanowires have pentagonal cross-sections, and one of the faces of the pentagon is blocked from the liquid for the supported nanowires. Comparing the quality factors for the supported and suspended nanowires in air also allows us to estimate the damping from the substrate. We find a relatively large quality factor of $\langle Q_{sub} \rangle = 240 \pm 40$. The value of $\langle Q_{sub} \rangle$ is much larger than the calculated values for nanowires in contact with a glass surface that assume continuity of stress and stain at the nanowire-solid interface. This is attributed to poor mechanical contact between the nanowires and the solid substrate in the experimental system, which means that the boundary conditions used in the calculations are not appropriate.

Conflict of Interest: No conflicts of interest exist for this paper.

Acknowledgements: This work was supported by the US National Science Foundation through grant CHE-1502848. KY acknowledges financial support from the National Natural Science Foundation of China (NSFC) (61705133) and the Science and Technology Innovation Commission of Shenzhen (JCYJ20170818143739628). DC and JES acknowledge support from the Australian Research Council Centre of Excellence in Exciton Science and the Australian Research Council Grants Scheme.

ORCID IDs:
Tuphan Devkota: 0000-0002-0572-5874
Kuai Yu: 0000-0001-6138-0367
Gary Beane: 0000-0001-5312-0477
Gregory V. Hartland: 0000-0002-8650-6891
John E. Sader: 0000-0002-7096-0627

References:

1. A. P. Alivisatos, *Science*, 1996, **271**, 933-937.
2. C. B. Murray, C. R. Kagan and M. G. Bawendi, *Annual Review of Materials Science*, 2000, **30**, 545-610.
3. Y. N. Xia, P. D. Yang, Y. G. Sun, Y. Y. Wu, B. Mayers, B. Gates, Y. D. Yin, F. Kim and Y. Q. Yan, *Advanced Materials*, 2003, **15**, 353-389.
4. C. Burda, X. B. Chen, R. Narayanan and M. A. El-Sayed, *Chemical Reviews*, 2005, **105**, 1025-1102.
5. Y. G. Sun and Y. N. Xia, *Science*, 2002, **298**, 2176-2179.
6. K. L. Kelly, E. Coronado, L. L. Zhao and G. C. Schatz, *J. Phys. Chem. B*, 2003, **107**, 668-677.
7. B. Wiley, Y. G. Sun, B. Mayers and Y. N. Xia, *Chem. Eur. J.*, 2005, **11**, 454-463.
8. R. C. Jin, *Nanoscale*, 2010, **2**, 343-362.
9. A. Crut, P. Maioli, N. Del Fatti and F. Vallee, *Phys. Rep.*, 2015, **549**, 1-43.
10. G. V. Hartland, *Chem. Rev.*, 2011, **111**, 3858-3887.
11. D. Chakraborty, G. V. Hartland, M. Pelton and J. E. Sader, *J. Phys. Chem. C*, 2017, DOI: 10.1021/acs.jpcc.7b09951, DOI: 10.1021/acs.jpcc.1027b09951.
12. M. Pelton, J. E. Sader, J. Burgin, M. Z. Liu, P. Guyot-Sionnest and D. Gosztola, *Nature Nanotech.*, 2009, **4**, 492-495.
13. M. Pelton, Y. Wang, D. Gosztola and J. E. Sader, *J. Phys. Chem. C*, 2011, **115**, 23732-23740.
14. M. Pelton, D. Chakraborty, E. Malachosky, P. Guyot-Sionnest and J. E. Sader, *Phys. Rev. Lett.*, 2013, **111**, 244502.
15. D. Chakraborty, E. van Leeuwen, M. Pelton and J. E. Sader, *J. Phys. Chem. C*, 2013, **117**, 8536-8544.
16. K. Yu, T. A. Major, D. Chakraborty, M. S. Devadas, J. E. Sader and G. V. Hartland, *Nano Letters*, 2015, **15**, 3964-3970.
17. D. Chakraborty and J. E. Sader, *Phys. Fluids*, 2015, **27**, 052002.
18. T. A. Major, A. Crut, B. Gao, S. S. Lo, N. D. Fatti, F. Vallee and G. V. Hartland, *Phys. Chem. Chem. Phys.*, 2013, **15**, 4169-4176.
19. M. A. van Dijk, M. Lippitz and M. Orrit, *Phys. Rev. Lett.*, 2005, **95**, 267406.
20. O. L. Muskens, N. Del Fatti and F. Vallee, *Nano Letters*, 2006, **6**, 552-556.
21. R. Marty, A. Arbouet, C. Girard, A. Mlayah, V. Paillard, V. K. Lin, S. L. Teo and S. Tripathy, *Nano Letters*, 2011, **11**, 3301-3306.
22. M. Dzida, E. Zorebski, M. Zorebski, M. Zarska, M. Geppert-Rybczynska, M. Chorazewski, J. Jacquemin and I. Cibulka, *Chem. Rev.*, 2017, **117**, 3883-3929.
23. L. Belliard, T. W. Cornelius, B. Perrin, N. Kacemi, L. Becerra, O. Thomas, M. E. Toimil-Molares and M. Cassinelli, *J. Appl. Phys.*, 2013, **114**, 193509.
24. C. Jean, L. Belliard, T. W. Cornelius, O. Thomas, M. E. Toimil-Molares, M. Cassinelli, L. Becerra and B. Perrin, *J. Phys. Chem. Lett.*, 2014, **5**, 4100-4104.
25. E. Gil-Santos, D. Ramos, J. Martinez, M. Fernandez-Regulez, R. Garcia, A. San Paulo, M. Calleja and J. Tamayo, *Nature Nanotechnology*, 2010, **5**, 641-645.
26. J. Lee, W. J. Shen, K. Payer, T. P. Burg and S. R. Manalis, *Nano Letters*, 2010, **10**, 2537-2542.

27. M. S. Devadas, T. Devkota, P. Johns, Z. M. Li, S. S. Lo, K. Yu, L. B. Huang and G. V. Hartland, *Nanotechnology*, 2015, **26**, 354001.
28. T. A. Major, S. S. Lo, K. Yu and G. V. Hartland, *J. Phys. Chem. Lett.*, 2014, **5**, 866-874.
29. G. D'Arrigo, *J. Chem. Phys.*, 1981, **75**, 921-928.
30. N.-S. Cheng, *Indust. Engin. Chem. Res.*, 2008, **47**, 3285-3288.
31. G. Hartland, *Journal of Chemical Physics*, 2002, **116**, 8048-8055.
32. N. Del Fatti, C. Voisin, F. Chevy, F. Vallee and C. Flytzanis, *J. Chem. Phys.*, 1999, **110**, 11484-11487.
33. C. Voisin, N. Del Fatti, D. Christofilos and F. Vallee, *J. Phys. Chem. B*, 2001, **105**, 2264-2280.
34. H. Staleva, S. E. Skrabalak, C. R. Carey, T. Kosel, Y. Xia and G. V. Hartland, *Phys. Chem. Chem. Phys.*, 2009, **11**, 5889-5896.
35. P. V. Ruijgrok, P. Zijlstra, A. L. Tchebotareva and M. Orrit, *Nano Letters*, 2012, **12**, 1063-1069.
36. K. Yu, P. Zijlstra, J. E. Sader, Q.-H. Xu and M. Orrit, *Nano Letters*, 2013, **13**, 2710-2716.
37. J. Burgin, P. Langot, N. Del Fatti, F. Vallee, W. Huang and M. A. El-Sayed, *J. Phys. Chem. C*, 2008, **112**, 11231-11235.
38. T. A. Kelf, Y. Tanaka, O. Matsuda, E. M. Larsson, D. S. Sutherland and O. B. Wright, *Nano Letters*, 2011, **11**, 3893-3898.
39. W. S. Chang, F. F. Wen, D. Chakraborty, M. N. Su, Y. Zhang, B. Shuang, P. Nordlander, J. E. Sader, N. J. Halas and S. Link, *Nature Commun.*, 2015, **6**, 7022.
40. M. N. Su, P. D. Dongare, D. Chakraborty, Y. Zhang, C. Y. Yi, F. F. Wen, W. S. Chang, P. Nordlander, J. E. Sader, N. J. Halas and S. Link, *Nano Letters*, 2017, **17**, 2575-2583.
41. J. Fedou, S. Viarbitskaya, R. Marty, J. Sharma, V. Paillard, E. Dujardin and A. Arbouet, *Phys. Chem. Chem. Phys.*, 2013, **15**, 4205-4213.
42. C. Yi, M.-N. Su, P. Dongare, D. Chakraborty, Y.-Y. Cai, D. M. Marolf, R. N. Kress, B. Ostovar, L. J. Tauzin, F. Wen, W.-S. Chang, M. Jones, J. E. Sader, N. J. Halas and S. Link, *Nano Letters*, 2018, DOI: 10.1021/acs.nanolett.8b00559.
43. V. A. Dubrovskiy and V. S. Morochnik, *Earth Phys.*, 1981, **17**, 494-504
44. A. Crut, V. Juve, D. Mongin, P. Maioli, N. Del Fatti and F. Vallee, *Phys. Rev. B*, 2011, **83**, 205430.
45. D. B. Murray and L. Saviot, *Phys Rev B*, 2004, **69**, 094305.
46. C. Jean, L. Belliard, T. W. Cornelius, O. Thomas, Y. Pennec, M. Cassinelli, M. E. Toimil-Molares and B. Perrin, *Nano Letters*, 2016, **16**, 6592-6598.
47. M. Hu, X. Wang, G. V. Hartland, P. Mulvaney, J. P. Juste and J. E. Sader, *J. Am. Chem. Soc.*, 2003, **125**, 14925-14933.
48. A. Crut, P. Maioli, N. Del Fatti and F. Vallee, *Phys. Chem. Chem. Phys.*, 2009, **11**, 5882-5888.
49. V. Kotaidis, T. Dekorsy, S. Ibrahimkutty, D. Issenmann, D. Khakhulin and A. Plech, *Phys Rev B*, 2012, **86**, 100101.
50. M. Hettich, K. Jacob, O. Ristow, C. He, J. Mayer, M. Schubert, V. Gusev, A. Bruchhausen and T. Dekorsy, *Applied Physics Letters*, 2012, **101**, 191606.
51. Y. Guillet, B. Audoin, M. Ferrie and S. Ravaine, *Phys. Rev. B*, 2012, **86**, 035456.

TOC Graphic:

Energy relaxation of the breathing modes of metal nanostructures is controlled by radiation of sound waves in the environment